Original Paper

Pathobiology

Pathobiology 2010;77:191–199
DOI: 10.1159/000292652

Received: December 23, 2009
Accepted after revision: February 5, 2010

Induction of GNE in Myofibers after Muscle Injury

Kenichiro Nakamura[a, b] Yoshiyuki Tsukamoto[a] Naoki Hijiya[a] Yasunori Higuchi[d]
Shinji Yano[c] Shigeo Yokoyama[c] Toshihide Kumamoto[b] Masatsugu Moriyama[a]

Departments of [a]Molecular Pathology, [b]Neurology and Neuromuscular Disorders Science, and [c]Diagnostic Pathology, Faculty of Medicine, Oita University, and [d]Research Center for Applied Medical Engineering, Oita University, Yufu City, Japan

Key Words
Uridine diphospho-N-acetylglucosamine 2-epimerase/N-acetylmannosamine kinase · Muscle · Regeneration

Abstract
Objective: The aim of the present study was to clarify the expression of uridine diphospho-N-acetylglucosamine 2-epimerase/N-acetylmannosamine kinase (GNE) protein and mRNA in damaged or regenerating myofibers. ***Methods:*** We investigated the muscle expression pattern of GNE protein by immunohistochemistry using a murine model involving intramuscular injection of cardiotoxin (CTX), and the expression level of GNE mRNA by quantitative real-time polymerase chain reaction analysis of damaged or regenerating myofibers that had been collected directly from tissue sections using laser-capture microdissection. ***Results:*** The expression of GNE protein was increased in severely damaged myofibers as well as in regenerating myofibers with central nuclei, both of which also showed an increase in the expression of GNE mRNA. In regenerating myofibers, immunoreactivity for GNE protein in nuclei relative to that in the cytoplasm was higher at 7 days than at 4 days after CTX injection. ***Conclusion:*** Our findings suggest that GNE expression is induced when myofibers are damaged or regenerating, and that GNE plays a role in muscle regeneration.

Introduction

The *GNE* gene encodes uridine diphospho-N-acetylglucosamine 2-epimerase/N-acetylmannosamine kinase (GNE), a key enzyme in the sialic acid biosynthetic pathway [1–3]. Sialic acids are expressed as terminal carbohydrates on glycoconjugates of eukaryotic cells, and function in cellular interactions and signaling [3, 4]. Under physiological conditions, GNE is expressed in various tissues, including muscle in mice as well as humans [5–7]. Deletion of the *GNE* gene in mice is embryonically lethal, suggesting that GNE plays an important role in development [8]. It is widely accepted that germ line mutation of the *GNE* gene is responsible for the pathogenesis of an autosomal recessive muscle disease with early adult onset, distal myopathy with rimmed vacuoles [9] and hereditary inclusion body myopathy [10]. Distal myopathy with rimmed vacuoles/hereditary inclusion body myopathy is characterized clinically by gradually progressive limb muscle weakness and atrophy, and pathologically by the presence of many cytoplasmic rimmed vacuoles, intranuclear tubulofilamentous inclusions and myofiber atrophy with little evidence of necrosis or regeneration [11–14]. It has recently been reported that the expression and subcellular distribution of GNE protein in muscle from patients with hereditary inclusion body myopathy are similar to those in normal muscle [15]. However, it is

KARGER
Fax +41 61 306 12 34
E-Mail karger@karger.ch
www.karger.com

1015–2008/10/0774–0191$26.00/0

Accessible online at:
www.karger.com/pat

Masatsugu Moriyama, MD, PhD
Department of Molecular Pathology
Faculty of Medicine, Oita University
Yufu City, Oita 879-5593 (Japan)
Tel. +81 97 586 5690, Fax +81 97 586 5699, E-Mail mmoriyam@med.oita-u.ac.jp

unknown whether the expression pattern of GNE in vivo changes in the regeneration process after muscle injury. In the present study, we investigated the expression pattern of GNE during the regeneration process after muscle injury induced by injection of cardiotoxin (CTX), and found that GNE is induced in both severely damaged myofibers and regenerating myofibers after muscle injury.

Materials and Methods

Animals and CTX Injection

C57BL/6 male mice (Kyudo, Saga, Japan) aged 7–12 weeks were used in this study. All experiments were performed in accordance with the guidelines for animal care and use at Oita University (Permission No. H008001). After anesthesia, 50 μl of 10 μM CTX (Latoxan, Rosans, France) was injected into the right gastrocnemius muscle. At 1, 2, 4, and 7 days after CTX injection, mice were sacrificed and the gastrocnemius muscles were resected. Muscles were fixed with 4% paraformaldehyde and embedded in paraffin, or immediately frozen in liquid nitrogen-cooled isopentane and stored at –80°C. Noninjected gastrocnemius muscles were used as control.

Generation of GNE Antibodies

Total RNA was extracted from a human monocytic leukemia cell line (THP-1). The cDNA fragment encoding the full length of the GNE protein was synthesized and amplified by reverse-transcription polymerase chain reaction (RT-PCR) with the forward primer 5′-ACCTCTCAAAACGAAACAAG-3′ and the reverse primer 5′-AAGAAACGGTCATCCTAAAG-3′. The PCR product was subcloned into pGEM-T easy vector (Promega, Madison, Wisc., USA) and sequenced (GNE-pGEM-T easy). Although plurally cloned cDNAs have the same mutation (A to G) at codon 309, we used this clone in the following experiment, since this mutation may not affect the amino acid sequence.

Next, in order to generate recombinant GNE protein fused to glutathione-S-transferase (GST), cDNAs encoding the N-terminal region (1–380 amino acids) of GNE (GNE-E) and the C-terminal region (410–722 amino acids) of GNE (GNE-K) were amplified by PCR with the following primers: GNE-E forward, 5′-CGCGGATCCATGGAGAAGAACGGGAAT; GNE-E reverse, 5′-CCGCTCGAGTCATGAAGGTCGATGGATTTG; GNE-K forward, 5′-CGCGGATCCTTGGCTGTTGATCTCGGG; GNE-K reverse, 5′-CCGCTCGAGCTAGTGGATCCTGCGGGT and GNE-pGEM-T easy as the template. Following sequencing, the cDNAs were subcloned into the *Bam*HI and *Xho*I sites of the pGEX4T-1 vector plasmid (Amersham Biosciences, Piscataway, N.J., USA), respectively. The construct of the full-length GNE fused to GST (GST-GNE) was done by cloning from GNE-pGEM-T easy to pGEX4T-1 at the *Eco*RI site. GST-GNE-E, GST-GNE-K and GST-GNE were synthesized and purified as described previously [16].

The purified GST-GNE-E and GST-GNE-K proteins were used to immunize rabbits to raise anti-GNE polyclonal antibodies. The antibodies were affinity purified as described previously [17]. The purified antibodies, designated 'α-GNE-E Ab' and 'α-GNE-K Ab' and directed at the GST-GNE-E and GST-GNE-K proteins, respectively, were used in the following experiments.

The additional primary and secondary antibodies listed in online supplementary table 1 (for all supplementary material, see www.karger.com/doi/10.1159/000292652) were obtained commercially and used according to the manufacturer's instructions.

Histological Analysis

The cross-sectional area (CSA) of the regenerating myofibers and the gastrocnemius muscle were measured using NIH ImageJ software. The CSA of the regenerating myofibers (μm^2) and the number of damaged or regenerating myofibers per unit CSA (mm^2) were expressed as means ± SD. Differences between variances were tested by the Mann-Whitney U test as a nonparametric method.

Immunohistochemistry and Double-Labeled Immunofluorescence

Immunohistochemistry and double-labeled immunofluorescence were performed as described previously [18]. Briefly, paraffin-embedded tissue sections were deparaffinized and rehydrated using standard protocols. Tissue sections from frozen specimens were fixed in 4% paraformaldehyde for 20 min at room temperature (RT). For antigen retrieval, sections were immersed in 10 mM sodium citrate buffer, pH 6.0 (Iatron, Tokyo, Japan), autoclaved at 120°C for 10 min and cooled to RT. They were treated with 3% H_2O_2 for 5 min at RT to inactivate endogenous peroxidase activity for avidin-biotin complex methods. After blocking with 10% goat serum (Nichirei, Tokyo, Japan) for 30 min at RT, immunohistochemistry with rabbit polyclonal α-GNE-K Ab was performed by incubating the tissue sections overnight at 4°C with the first antibody at concentrations of 4 μg/ml in diluting solution (Dako, Copenhagen, Denmark).

For avidin-biotin complex methods, the sections were then washed with 1 × phosphate-buffered saline (PBS) and incubated for 30 min with biotinylated goat α-rabbit IgG antibody (Nichirei). After being washed, they were incubated with a solution of avidin-conjugated horseradish peroxidase (Vectastain Elite ABC kit; Vector Laboratories Inc., Burlingame, Calif., USA) for 15 min, according to the manufacturer's recommendations, and then washed. Peroxidase activity was detected with H_2O_2/diaminobenzidine substrate solution, and the sections were counterstained with hematoxylin before dehydration and mounting.

For double-labeled immunofluorescence, sections incubated with a mixture of appropriately diluted first antibodies were then washed with 1 × PBS and incubated with a mixture of appropriately diluted secondary antibodies or propidium iodide (Sigma, Tokyo, Japan) for 2 h at RT. They were then washed and mounted. The mounted sections were observed using the LSM5 Pascal confocal laser scanning microscope (Carl Zeiss, Oberkochen, Germany).

For antigen competition experiments, prior to immunostaining α-GNE-K Ab was preabsorbed to more than a 700-fold weight excess of GST-GNE-K.

Western Blotting

Fresh-frozen samples were ground to a fine powder with liquid nitrogen. Total proteins were extracted as described previously [19]. Western blotting analysis was performed as described previously [20].

Extraction of Total RNA from Laser-Capture Microdissected Myofiber Samples

Tissue sections 10 μm thick were cut from frozen blocks with a cryostat Leica CM1850 (Leica Microsystems, Wetzlar, Germany), and then stained with cresyl violet (Ambion). Damaged, regenerating or control myofibers were collected from the tissue sections using the Arcturus^{XT} microdissection system (Arcturus Engineering Inc., Mountain View, Calif., USA). Control myofibers (with a normal appearance) were collected from the same tissue sections from which damaged or regenerating myofibers had also been collected. The collected myofibers were dissolved immediately in Isogen reagent (Nippon Gene, Tokyo, Japan), and total RNA was isolated as described by the manufacturer. Reverse transcription was carried out using a Transcriptor first-strand cDNA synthesis kit (Roche, Mannheim, Germany) with random hexamer primers, in accordance with the manufacturer's instructions.

Quantitative PCR for GNE

Quantitative real time PCR (qRT-PCR) was performed using LightCycler FastStart DNA Master SYBR Green I (Roche, Mannheim, Germany) and analyzed in a LightCycler 2.0 (Roche) with LightCycler Software version 4.0 (Roche), according to the manufacturer's instructions. Primers for mouse GNE (MA065432) (forward, 5′-ACGTGAAGGCCCAGAGCATC; reverse, 5′-TGACTGGCCAGGACTCCAGA) and mouse GAPDH (MA050371) (forward, 5′-TGTGTCCGTCGTGGATCTGA; reverse, 5′-TTGCTGTTGAAGTCGCAGGAG) were designed by and purchased from Takarabio (Shiga, Japan). Dilutions of cDNA synthesized from noninjected murine gastrocnemius muscles were used as standards. qRT-PCR was carried out using the following cycle parameters: 1 cycle of 10 min at 95°C, followed by 40 cycles of 10 s at 95°C, 10 s at 60°C, and 20 s at 72°C. Melting curve analysis was performed to confirm the correct PCR product. GAPDH was used as a control and relative expression levels were obtained by relative quantification analysis. PCR amplification was duplicated in independent experiments.

Immunoelectron Microscopy

The gastrocnemius muscles at 7 days after CTX injection were fixed in 4% paraformaldehyde overnight, followed by routine embedding in paraffin. Tissue sections stained with hematoxylin and eosin (HE) were then prepared and observed by light microscopy, and we selectively obtained tissues that were rich in regenerating myofibers. The selected tissues were cut into small pieces with a knife, deparaffinized in xylene, rehydrated in ethanol, and fixed overnight at 4°C in a mixture of 2% paraformaldehyde, 0.5% glutaraldehyde, 0.2 mM $CaCl_2$, and 0.1 mM $MgCl_2$ in 0.1 M sodium cacodylate buffer, pH 7.4, which was supplemented with tannic acid at a final concentration of 0.1%, just before use. The pieces were dehydrated in an ascending graded ethanol series and infiltrated with LR White resin (London Resin Company, UK), which was polymerized by heating at 55°C for 24 h. LR White-embedded blocks for immunoelectron microscopy using α-GNE-K Ab were prepared as described previously [18, 21]. Briefly, ultrathin sections were cut with an ultramicrotome (Leica Instruments, Nussloch, Germany) at a thickness of 90 nm and mounted on nickel grids that had been coated with carbon in a vacuum evaporator. For immunostaining, nickel grids bearing sections were immersed in an alkaline solution (Target Retrieval Solution, pH 10; Dako, Carpinteria, Calif., USA), heated at 95°C for 30 min, and then cooled to RT. After blocking, the sections were incubated with α-GNE-K Ab (5 μg/ml) diluted with 1 × Tris-buffered saline containing 0.1% (w/v) bovine serum albumin at 4°C for 18 h. After washing, the sections were incubated with the appropriately diluted 15-nm gold particle-conjugated secondary antibody at RT for 30 min. After washing, the sections were counterstained with uranyl acetate and lead citrate, and observed with a transmission electron microscope (JEM 1230, Jeol Ltd., Tokyo, Japan). Preparations of normal quadriceps muscle were made in a similar way. Negative controls were prepared by omitting the first antibody.

Results

Characterization of Anti-GNE Antibodies

We generated two affinity-purified anti-GNE antibodies by immunizing rabbits with the recombinant GNE protein fused to GST containing the epimerase domain corresponding to amino acids 1–380 (GNE-E), or with that containing the kinase domain corresponding to amino acids 410–722 (GNE-K), as described in Materials and Methods (online suppl. fig. 1A). On Western blots, while α-GNE-E Ab and α-GNE-K Ab were specifically immunoreactive with GNE-E and GNE-K, respectively (online suppl. fig. 1B), both of the antibodies were immunoreactive with purified full-length GNE proteins fused to GST (online suppl. fig. 1B) as well as with full-length GNE proteins fused to GFP exogenously expressed in HEK293 cells (online suppl. fig. 1C). As shown in online supplementary figure 1D, Western blotting analysis of extracts from the murine muscle tissue showed that both α-GNE-E Ab and α-GNE-K Ab detected a band at about 79 kDa corresponding to GNE [7]. Immunohistochemical analysis of the normal murine muscle showed that positive immunoreactivity for α-GNE-K Ab was detected mainly in the cytoplasm and occasionally in the nuclei of myofibers (fig. 1A). Nonspecific immunoreactivity was unlikely because these positive immunoreactivities were found to be significantly decreased in the antigen competition experiments (fig. 1B). Double-labeled immunohistochemistry with α-GNE-K Ab showed that the expression of GNE protein overlapped with that of α-actinin (online suppl. fig. 1E–G), in accord with the findings of a previous study [22]. Immunoelectron microscopy analysis of normal murine muscle with α-GNE-K Ab showed that immunolabeled gold particles were attached to the sarcomeric Z-lines and I-bands (fig. 2A).

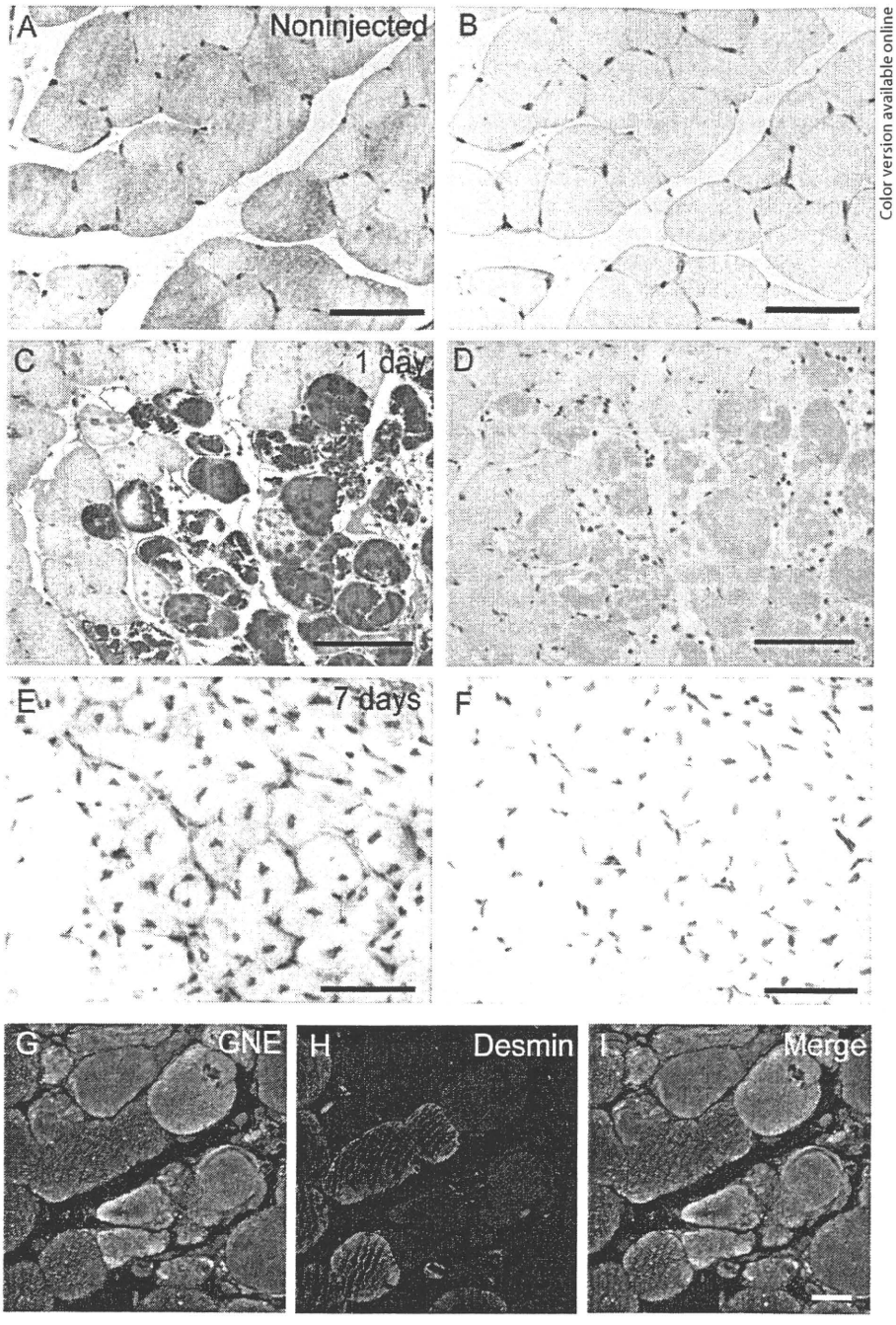

Fig. 1. Immunohistochemical analysis of GNE in CTX-injected murine gastrocnemius muscles. **A–F** Paraffin-embedded tissue sections from noninjected murine gastrocnemius muscles (**A**, **B**), and at 1 day (**C**, **D**) and 7 days (**E**, **F**) after CTX injection were immunostained with α-GNE-K Ab. Positive immunoreactivity (**A**, **C**, **E**) is significantly decreased in competition experiments (**B**, **D**, **F**). **G–I** Tissue sections from murine gastrocnemius muscles at 2 days after CTX injection were analyzed by double-labeled immunostaining analysis with α-GNE-K Ab (green) together with α-desmin antibody (red). Immunoreactivity for desmin is positive in viable myofibers and negative in damaged myofibers. Results were similar in at least 3 independent experiments. Scale bars: 50 μm (**A**, **B**, **E**, **F**), 100 μm (**C**, **D**) and 20 μm (**I**).

Expression of GNE Protein Is Increased in Damaged or Regenerating Myofibers of CTX-Injected Mice

To determine whether the expression pattern of GNE is changed during the process of regeneration after muscle injury, we investigated the expression pattern of GNE in the gastrocnemius muscle after intramuscular injection of CTX. In accordance with previous reports [23, 24], histological analysis showed that many destroyed or damaged myofibers were present at 1 and 2 days after CTX injection (online suppl. fig. 2A, B). At 4 days after CTX injection, while the number of damaged myofibers had decreased (38.1 ± 5.8, 39.1 ± 7.4, and 1.1 ± 1.2 myofibers per square millimeter CSA at 1, 2, and 4 days after CTX injection, respectively, n = 3, p = 0.04), basophilic regenerating myofibers with central nuclei were present together with small mononuclear cells, probably includ-

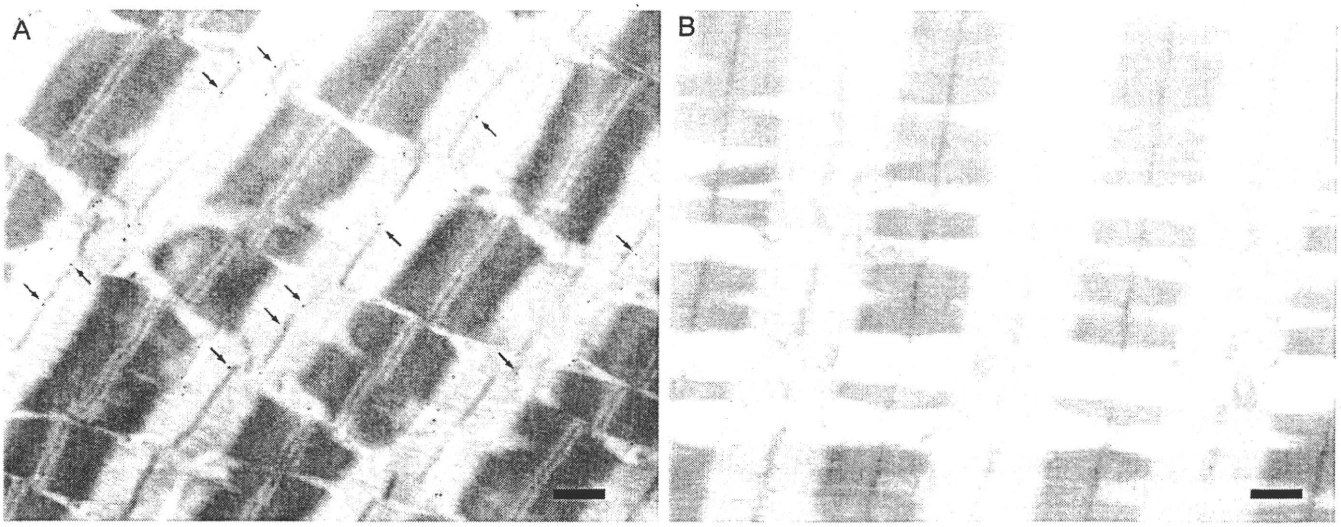

Fig. 2. Immunoelectron microscopy analysis of normal murine quadriceps muscle using α-GNE-K Ab (**A**), and a negative control omitting the first antibody (**B**). Arrows indicate GNE protein localized to the Z-line. Scale bar: 0.5 μm.

ing activated satellite cells, fibroblasts and macrophages (online suppl. fig. 2C). At 7 days after CTX injection, the number of regenerating myofibers with central nuclei had increased (79.3 ± 31.1 and 188.5 ± 69.6 myofibers per square millimeter CSA at 4 and 7 days after CTX injection, respectively, n = 4, p = 0.02) (online suppl. fig. 2D).

Immunohistochemical analysis demonstrated strongly positive immunoreactivity with α-GNE-K Ab in myofibers corresponding to those that had been found to be damaged on histological analysis 1 and 2 days after CTX injection (fig. 1C). This positive immunoreactivity was significantly decreased by antigen competition (fig. 1D). Double-labeled immunohistochemistry demonstrated that desmin was downregulated in myofibers that were strongly GNE positive (fig. 1G–I), suggesting that these myofibers were severely damaged [25–29]. Furthermore, Western blotting analysis revealed that the expression level of GNE protein was significantly increased at 1 and 2 days after CTX injection (online suppl. fig. 3).

Positive immunoreactivity for α-GNE-K Ab was also detected in both the cytoplasm and the central nuclei of regenerating myofibers at 7 days after CTX injection, and the immunoreactivity in regenerating myofibers was stronger than that in nondamaged mature myofibers with peripheral nuclei (fig. 1E). This immunoreactivity was significantly decreased by antigen competition (fig. 1F). We found that the immunoreactivity for GNE protein in the nuclei relative to that in the cytoplasm of regenerating myofibers was higher at 7 days than at 4 days after CTX injection (fig. 3A–F). The CSA of regenerating myofibers was significantly increased at 7 days (492.1 ± 193.4 μm^2, 276 myofibers) compared with that at 4 days (188.0 ± 72.5 μm^2, 263 myofibers) after CTX injection ($p < 0.0001$). Double-labeled immunohistochemistry showed that some small mononuclear cells expressing GNE coexpressed myogenin (fig. 3G–L), suggesting a population of activated satellite cells.

Immunoelectron microscopy analysis using α-GNE-K Ab showed immunolabeled gold particles attached to the central nucleus; immunolabeled gold particles were also present in the cytoplasm of regenerating myofibers at 7 days after CTX injection (fig. 4A, B). Positive signals were not distributed diffusely in the nucleus but were detectable in the peripheral heterochromatin (fig. 4B) as well as internal electron-dense regions (fig. 4B). Furthermore, positive signals were also detectable at the nucleolus (fig. 4B).

Induction of GNE in Damaged or Regenerating Myofibers Confirmed by qRT-PCR

To confirm the induction of GNE in damaged or regenerating myofibers, we selectively collected damaged or regenerating myofibers from sections of CTX-injured muscle tissue using laser-capture microdissection, and then measured the expression level of GNE mRNA by qRT-PCR analysis. Consistent with the immunohistochemical data (fig. 1C), the expression level of GNE mRNA in damaged myofibers was evidently increased in

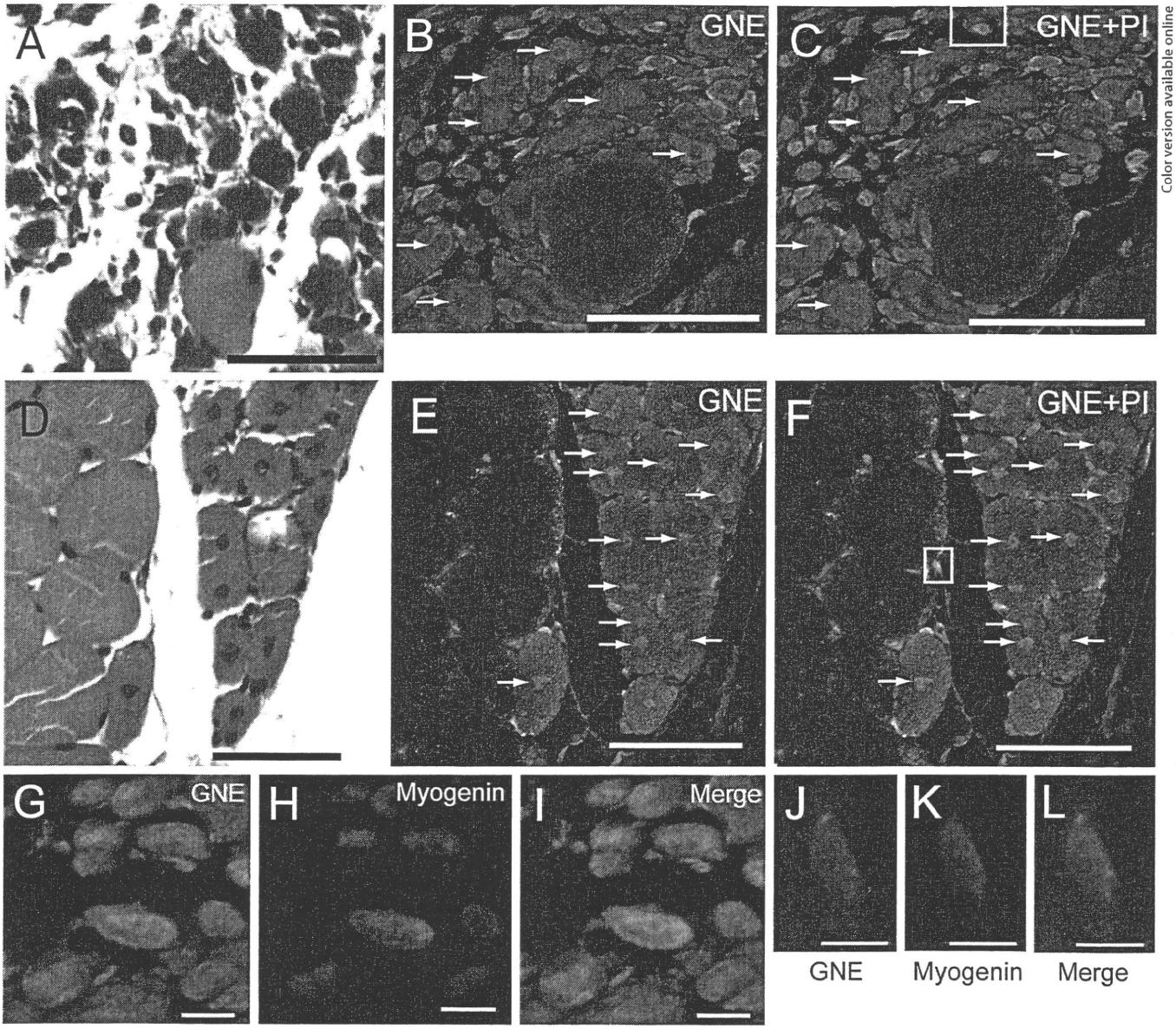

Fig. 3. Double-labeled immunofluorescence of GNE in regenerating muscle. Tissue sections from murine gastrocnemius muscles at 4 days (**A–C** and **G–I**) and 7 days (**D–F**, **J–L**) after CTX injection were stained by HE (**A**, **D**), immunostaining with α-GNE-K Ab (green) and nuclear staining (red) with propidium iodide (PI) after the sections had been incubated with ribonuclease (Sigma, Tokyo, Japan) (**B**, **C**, **E**, **F**), and double-labeled immunostaining with α-GNE-K Ab (green) together with α-myogenin antibody (red) (**G–L**). **G–I** and **J–L** correspond to the boxed areas in **C** and **F**, respectively. Arrows indicate central nuclei in regenerating myofibers. Scale bars: 50 μm (**A–F**) and 5 μm (**G–L**).

comparison with that in nondamaged myofibers (fig. 5A). Furthermore, the expression level of GNE mRNA in regenerating myofibers was also increased in comparison with that in control myofibers (fig. 5B). Thus, we concluded that GNE is induced in both damaged and regenerating myofibers.

Discussion

We found that the expression level of GNE was increased in damaged and regenerating myofibers. GNE was inducible not only by intramuscular injection of CTX but also by touching the muscle with dry ice (data not

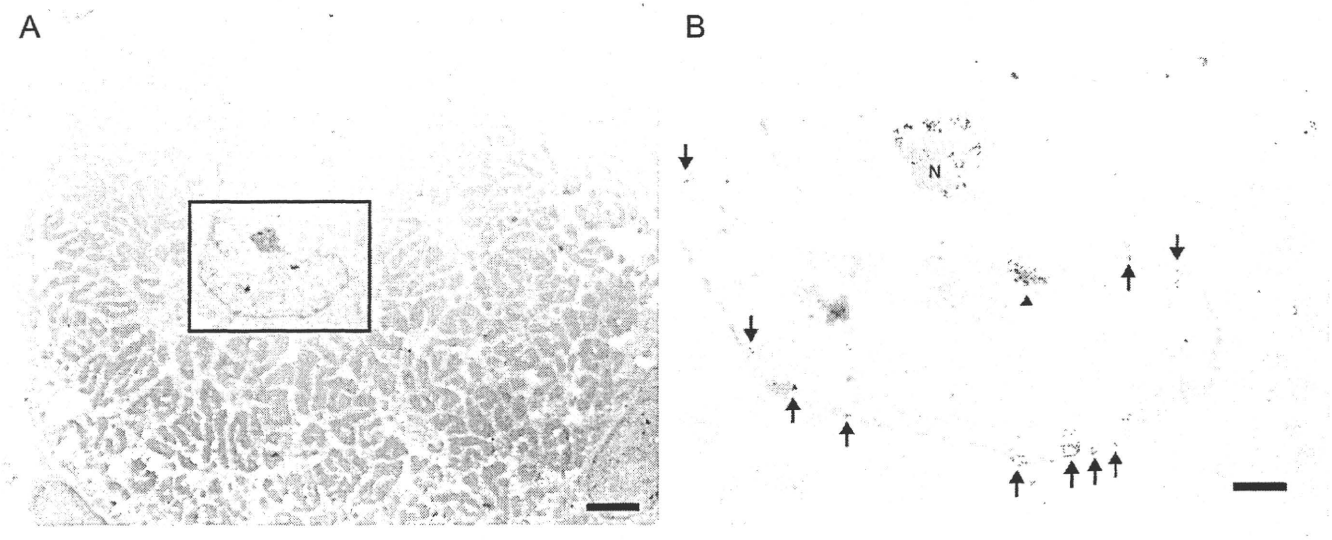

Fig. 4. Immunoelectron microscopy analysis of GNE in regenerating myofibers at 7 days after CTX injection. **A** A representative regenerating myofiber with a central nucleus. **B** High-power view of the boxed area in **A**. The arrowhead indicates the internal electron-dense region. Arrows indicate the peripheral heterochromatin. N = Nucleolus. Scale bars: 2 μm (**A**) and 0.5 μm (**B**).

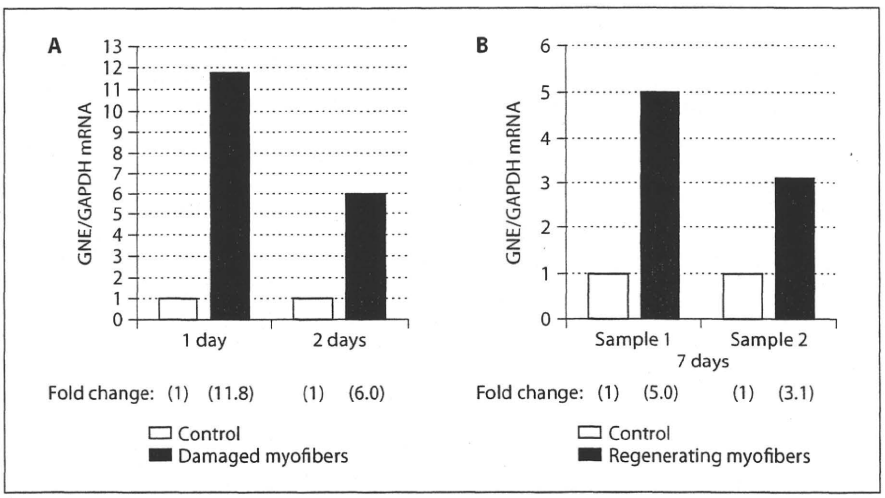

Fig. 5. Upregulation of GNE mRNA in damaged or regenerating myofibers. Damaged myofibers at 1 day and 2 days after CTX injection (**A**) and regenerating myofibers at 7 days after CTX injection (**B**) were selectively collected using laser-capture microdissection. The expression levels of GNE mRNA in damaged myo-fibers (**A**) and regenerating myofibers (**B**) were analyzed by qRT-PCR, and expressed as the fold change compared with the control (nondamaged myofibers). GAPDH mRNA was used as an internal control.

shown), suggesting that induction of GNE is not specific to CTX but rather can be induced by various kinds of muscle damage.

We showed that not only the expression level of GNE mRNA but also that of GNE protein was increased in damaged myofibers showing downregulation of desmin. Proteolysis is usually activated in damaged myofibers [28, 29]. Nevertheless, upregulation of some proteins, such as calcium-dependent proteinase, calpain, and its endogenous inhibitor calpastatin [30, 31], proteasomes [32], Bcl-2 and Bax [33], has been reported in necrotic myofibers. Myofibrillar protein degradation in CTX-induced myonecrosis, for example, is compatible with the 'two-step' mechanism; the first stage is associated with cytosolic muscle proteinases, mainly calpains, responsible for limited proteolysis of a few key structural proteins such as desmin; the second stage predominantly involves leukocyte and macrophage proteinases, which cause

widespread degradation of the most abundant myofibrillar components [28, 29]. These results suggest that proteolysis in damaged myofibers is not uniform. We speculate that GNE protein in damaged myofibers is stable, at least in comparison with desmin. Future studies of the mechanism responsible for degradation of GNE protein will help answer this question.

Neural cell adhesion molecules (NCAM) are reported to be polysialylated in regenerating myofibers in vivo and in myotubes in vitro [34, 35], suggesting that sialic acid has a role in muscle regeneration. It has also been reported that a polysialylated form of NCAM (PSA-NCAM) is expressed in regenerating myofibers as well as activated satellite cells after muscle injury induced by sodium dihydrogen phosphate [36]. In this model, the regeneration process is similar to that induced by CTX. PSA-NCAM is reported to be associated with cell rearrangement and migration during development [37]. However, the role of PSA-NCAM in muscle regeneration remains to be elucidated. It has recently been reported that polysialylation of NCAM is reduced in the brain of heterozygous GNE-deficient mice [38] as well as in GNE-deficient mouse embryonic stem cells [8]. Therefore, we speculate that GNE is induced and contributes to the regulation of sialic acid biosynthesis in regenerating myofibers.

In addition, we found that GNE protein was markedly localized in nuclei of regenerating myofibers at 7 days, as compared with that at 4 days after CTX injection, suggesting that the function of GNE alters during the regeneration process. The mechanism responsible for the nuclear localization of GNE is still unclear, although its translocation from the cytoplasm to the nucleus may be dependent upon some intracellular signaling process. Alternatively, the relative stability of the protein may differ between the nucleus and the cytoplasm in regenerating myofibers. It has recently been reported that promyelocytic leukemia zinc finger protein (PLZF) binds to GNE [39]. PLZF is a sequence-specific DNA-binding transcriptional repressor associated with corepressor molecules such as N-CoR, Sin3A, SMRT and HDAC1 [40–43]. It has already been reported that the cytoplasmic enzyme glyceraldehyde-3-phosphate dehydrogenase translocates to the nucleus in response to oxidative stress and associates with the regulator of transcription factors, APE1 [44]. Therefore, we speculate that GNE functions as a transcriptional regulator in regenerating myofibers via binding to such corepressor complexes.

Acknowledgments

This research was supported in part by the Ministry of Education, Science, Sports and Culture, Grant-in-Aid for Scientific Research (C), No. 15590898 and No. 18590952 and by Research on intractable diseases, Health and Labour Sciences Research Grants from the Ministry of Health, Labour and Welfare, Japan. We are grateful to Tsuyoshi Iwao, Mariko Ono and Kaori Hirano for excellent technical assistance.

References

1 Hinderlich S, Stäsche R, Zeitler R, Reutter W: A bifunctional enzyme catalyzes the first two steps in N-acetylneuraminic acid biosynthesis of rat liver. Purification and characterization of UDP-N-acetylglucosamine 2-epimerase/N-acetylmannosamine kinase. J Biol Chem 1997;272:24313–24318.

2 Stäsche R, Hinderlich S, Weise C, et al: A bifunctional enzyme catalyzes the first two steps in N-acetylneuraminic acid biosynthesis of rat liver. Molecular cloning and functional expression of UDP-N-acetylglucosamine 2-epimerase/N-acetylmannosamine kinase. J Biol Chem 1997;272:24319–24324.

3 Keppler OT, Hinderlich S, Langner J, Schwartz-Albiez R, Reutter W, Pawlita M: UDP-GlcNAc 2-epimerase: a regulator of cell surface sialylation. Science 1999;284:1372–1376.

4 Tanner ME: The enzymes of sialic acid biosynthesis. Bioorg Chem 2005;33:216–228.

5 Horstkorte R, Nöhring S, Wieschens N, et al: Tissue expression and amino acid sequence of murine UDP-N-acetylglucosamine 2-epimerase/N-acetylmannosamine kinase. Eur J Biochem 1999;260:923–927.

6 Lucka L, Krause M, Danker K, Reutter W, Horstkorte R: Primary structure and expression analysis of human UDP-N-acetylglucosamine 2-epimerase/N-acetylmannosamine kinase, the bifunctional enzyme in neuraminic acid biosynthesis. FEBS Lett 1999;454:341–344.

7 Krause S, Hinderlich S, Amsili S, et al: Localization of UDP-GlcNAc 2-epimerase/ManAc kinase (GNE) in the Golgi complex and the nucleus of mammalian cells. Exp Cell Res 2005;304:365–379.

8 Schwarzkopf M, Knobeloch K, Rohde E, Hinderlich S, Wiechens N, Lucka L, Horak I, Reutter W, Horstkorte R: Sialylation is essential for early development in mice. Proc Natl Acad Sci USA 2002;99:5267–5270.

9 Nishino I, Noguchi S, Murayama K, et al: Distal myopathy with rimmed vacuoles is allelic to hereditary inclusion body myopathy. Neurology 2002;59:1689–1693.

10 Eisenberg I, Avidan N, Potikha T, et al: The UDP-N-acetylglucosamine 2-epimerase/N-acetylmannosamine kinase gene is mutated in recessive hereditary inclusion body myopathy. Nat Genet 2001;29:83–87.

11 Nonaka I, Sunohara N, Ishiura S, Satoyoshi E: Familial distal myopathy with rimmed vacuole and lamellar (myeloid) body formation. J Neurol Sci 1981;51:141–155.

12 Kumamoto T, Fukuhara N, Nagashima M, Kanda T, Wakabayashi M: Distal myopathy: histochemical and ultrastructural studies. Arch Neurol 1982;39:367–371.

13 Argov Z, Yarom R: 'Rimmed vacuole myopathy' sparing the quadriceps: a unique disorder in Iranian Jews. J Neurol Sci 1984;64:33–43.

14 Nonaka I, Murakami N, Suzuki Y, Kawai M: Distal myopathy with rimmed vacuoles. Neuromuscul Disord 1998;8:333–337.
15 Krause S, Aleo A, Hinderlich S, et al: GNE protein expression and subcellular distribution are unaltered in HIBM. Neurology 2007; 69:655–659.
16 Onizuka T, Moriyama M, Yamauchi T, et al: BCL-6 Gene Product, a 92- to 98-kD nuclear phosphoprotein, is highly expressed in germinal center B cells and their neoplastic counterparts. Blood 1995;86:28–37.
17 Moriyama M, Tsukamoto Y, Fujiwara M, et al: Identification of a novel human ankyrin-repeated protein homologous to CARP. Biochem Biophys Res Commun 2001;285:715–723.
18 Tsukamoto Y, Hijiya N, Yano S, et al: Arpp/Ankrd2, a member of the muscle ankyrin repreat proteins (MARPs), translocates from the I-band to the nucleus after muscle injury. Histochem Cell Biol 2008;129:55–64.
19 Nakada C, Tsukamoto Y, Oka A, et al: Cardiac-restricted ankyrin-repeated protein is differentially induced in Duchenne and congenital muscular dystrophy. Lab Invest 2003; 83:711–719.
20 Uchida T, Kanada R, Tsukamoto Y, et al: Immunohistochemical diagnosis of the cagA-gene genotype of *Helicobacter pylori* with anti-East Asian CagA-specific antibody. Cancer Sci 2007;98:521–528.
21 Yano S, Kashima K, Daa T, et al: An antigen retrieval method using an alkaline solution allows immunoelectron microscopic identification of secretory granules in conventional epoxy-embedded tissue sections. J Histochem Cytochem 2003;51:199–204.
22 Amsili S, Zer H, Hinderlich S, et al: UDP-N-acetylglucosamine 2-epimerase/N-acetylmannosamine kinase (GNE) binds to α-actinin 1: novel pathways in skeletal muscle? PLoS One 2008;3:e2477.
23 Yan Z, Choi S, Liu X, et al: Highly coordinated gene regulation in mouse skeletal muscle regeneration. J Biol Chem 2003;278: 8826–8836.
24 Chargé SBP, Rudnicki MA: Cellular and molecular regeneration of muscle regeneration. Physiol Rev 2004;84:209–238.
25 Helliwell TR: Lectin binding and desmin staining during bupivacaine-induced necrosis and regeneration in rat skeletal muscle. J Pathol 1988;155:317–326.
26 Barash IA, Peters D, Fridén J, Lutz GJ, Lieber RL: Desmin cytoskeletal modifications after a bout of eccentric exercise in the rat. Am J Physiol Regul Integr Comp Physiol 2002; 283:R958–R963.
27 Lovering RM, DeDeyne PG: Contractile function, sarcolemma integrity, and the loss of dystrophin after skeletal muscle eccentric contraction-induced injury. Am J Physiol Cell Physiol 2004;286:C230–C238.
28 Gutiérrez JM, Ownby CL: Skeletal muscle degeneration induced by venom phospholipases A_2: insights into the mechanisms of local and systemic myotoxicity. Toxicon 2003; 42:915–931.
29 Harris JB, Vater R, Wilson M, Cullen MJ: Muscle fibre breakdown in venom-induced muscle degeneration. J Anat 2003;202:363–372.
30 Kumamoto T, Ueyama H, Watanabe S, et al: Immunohistochemical study of calpain and its endogenous inhibitor in the skeletal muscle of muscular dystrophy. Acta Neuropathol 1995;89:399–403.
31 Sultan KR, Dittrich BT, Leisner E, Paul N, Pette D: Fiber type-specific expression of major proteolytic systems in fast- to slow-transforming rabbit muscle. Am J Physiol Cell Physiol 2001;280:239–247.
32 Kumamoto T, Fujimoto S, Ito T, Horinouchi H, Ueyama H, Tsuda T: Proteasome expression in the skeletal muscles of patients with muscular dystrophy. Acta Neuropathol 2000;100:595–602.
33 Olivé M, Ferrer I: Bcl-2 and Bax protein expression in human myopathies. J Neurol Sci 1999;164:76–81.
34 Dubois C, Figarella-Branger D, Pastoret C, Rampini C, Karpati G, Rougon G: Expression of NCAM and its polysialylated isoforms during mdx mouse muscle regeneration and in vitro myogenesis. Neuromuscul Disord 1994;4:171–182.
35 Suzuki M, Angata K, Nakayama J, Fukuda M: Polysialic acid and mucin type *o*-glycans on the neural cell adhesion molecule differentially regulate myoblast fusion. J Biol Chem 2003;278:49459–49468.
36 Figarella-Branger D, Pellissier JF, Bianco N, Karpati G: Sequence of expression of MyoD1 and various cell surface and cytoskeletal proteins in regenerating mouse muscle fibers following treatment with sodium dihydrogen phosphate. J Neurol Sci 1999;170:151–160.
37 Rutishauser U: Polysialic acid at the cell surface: biophysics in service of cell interactions and tissue plasticity. J Cell Biochem 1998;70: 304–312.
38 Gagiannis D, Orthmann A, Danssmann I, Schwarzkopf M, Weidemann W, Horstkorte R: Reduced sialylation status in UDP-N-acetylglucosamine-2-epimerase/N-acetylmannosamine kinase (GNE)-deficient mice. Glycoconj J 2007;24:125–130.
39 Weidemann W, Stelzl U, Lisewski U, et al: The collapsin response mediator protein 1 (CRMP-1) and the promyelocytic leukemia zinc finger protein (PLZF) bind to UDP-N-acetylglucosamine 2-epimerase/N-acetylmannosamine kinase (GNE), the key enzyme of sialic acid biosynthesis. FEBS Lett 2006;580:6649–6654.
40 Li JY, English MA, Ball HJ, Yeyati PL, Waxman S, Licht JD: Sequence-specific DNA binding and transcriptional regulation by the promyelocytic leukemia zinc finger protein. J Biol Chem 1997;272:22447–22455.
41 Grignani F, Matteis SD, Nervi C, et al: Fusion proteins of the retinotic acid receptor-α recruit histone deacetylase in promyelocytic leukemia. Nature 1998;391:815–818.
42 Lin RJ, Nagy L, Inoue S, Shao W, Miller WH Jr, Evans RM: Role of the histone deacetylase complex in acute promyelocytic leukemia. Nature 1998;391:811–814.
43 Melnick AM, Westendorf JJ, Polinger A, et al: The ETO protein disrupted in t(8;21)-associated acute myeloid leukemia is a corepressor for the promyelocytic leukemia zinc finger protein. Mol Cell Biol 2000;20:2075–2086.
44 Azam S, Jouvet N, Jilani A, et al: Human glyceraldehyde-3-phosphate dehydrogenase plays a direct role in reactivating oxidized forms of the DNA repair enzyme APE1. J Biol Chem 2008;283:30632–30641.

Neurol Med Chir (Tokyo) 50, 336～338, 2010

Cerebral Vasculitis Associated With Amyloid Angiopathy

—Case Report—

Masaki MORISHIGE, Tatsuya ABE, Tohru KAMIDA, Takamitsu HIKAWA, Minoru FUJIKI, Hidenori KOBAYASHI, Toshiro OKAZAKI*, Noriyuki KIMURA*, Toshihide KUMAMOTO*, Akira YAMADA**, and Yoshihisa KAWANO**

*Departments of Neurosurgery and *Neurology, Oita University School of Medicine, Yufu, Oita; **Kawano Neurosurgical Hospital, Oita*

Abstract

A 78-year-old female presented with coexisting primary angiitis of the central nervous system (CNS) and cerebral amyloid angiopathy (CAA) manifesting as motor aphasia caused by a left frontal lobe lesion. Magnetic resonance imaging revealed an enhanced lesion with moderate surrounding edema.Technetium-99m propylene amine oxime single-photon emission computed tomography showed decreased cerebral blood flow (CBF) in the lesions, and high serum soluble-interleukin-2 level was detected, suggesting intravascular lymphoma of the CNS. Cerebral biopsy revealed CAA with secondary florid vasculitic appearance. The CBF and neurological symptoms, such as aphasia and dementia, recovered following steroid treatment. Cerebral vasculitis associated with CAA should be included in the differential diagnosis of an unusually enhanced lesion, because timely diagnosis and aggressive treatment are critical to successful recovery in such elderly patients.

Key words: brain tumor, vasculitis, cerebral amyloid angiopathy

Introduction

Cerebral amyloid angiopathy (CAA) occasionally coexists with cerebral vasculitis, including granulomatous angiitis (giant cell arteritis) of the brain. Such angiitis may cause amyloid deposition or vascular amyloid deposition may secondarily induce granulomatous (giant cell) reaction.[11] Primary angiitis of the central nervous system (CNS) is a serious type of inflammatory angiitis that only affects the CNS vessels in the absence of an overt systemic inflammatory process.[1] Early aggressive immunosuppressive therapy substantially improves the outcome but may also result in significant complications, so cerebral biopsy is indicated to rule out other conditions that mimic or cause CNS vasculitis.[3] We treated a patient with CAA mimicking a brain tumor.

Case Report

A 78-year-old female was admitted due to symptoms of motor aphasia and dementia. Magnetic resonance (MR) imaging demonstrated large confluent hyperintense areas predominantly in the white matter on T_2-weighted or fluid-attenuated inversion recovery images (Fig. 1A). T_1-weighted MR imaging with contrast medium showed decreased intensity with mild parenchymal enhancement in the left frontal lobe (Fig. 1B–D), consistent with either

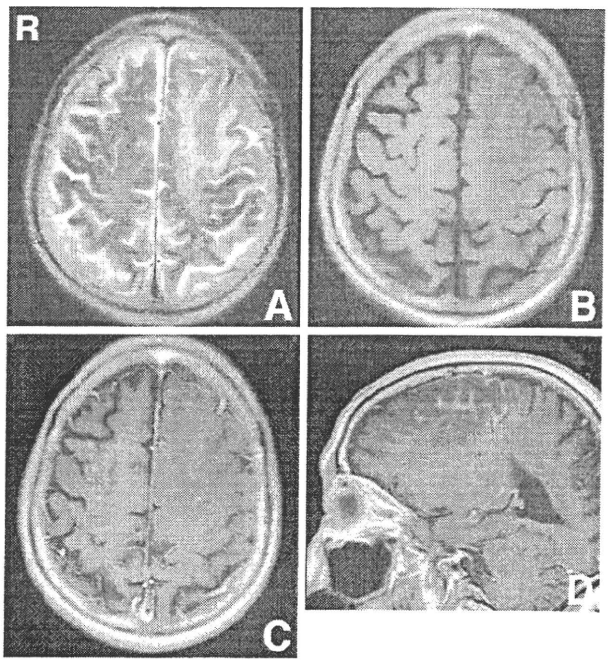

Fig. 1 (A) Preoperative T_2-weighted magnetic resonance (MR) image demonstrating a high intensity lesion in the left frontal lobe. (B) Preoperative T_1-weighted MR image demonstrating a low intensity lesion. (C, D) T_1-weighted MR images with gadolinium showing mildly enhanced lesions.

Received June 9, 2009; Accepted August 25, 2009

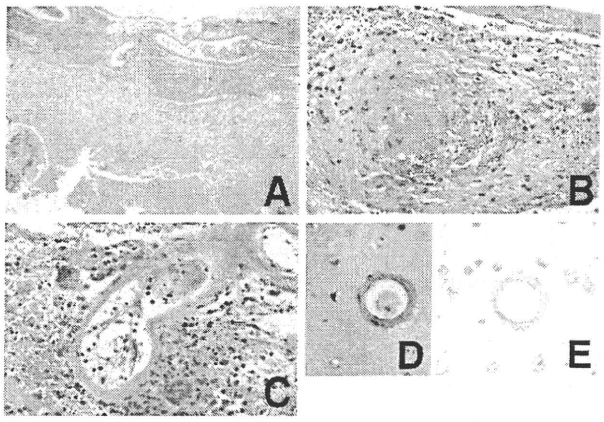

Fig. 2 Photomicrographs showing leptomeningeal infiltration of lymphocytes (A: hematoxylin and eosin [HE] stain, ×40), angiitis with transmural inflammation and fibrinoid necrosis (B: HE stain, ×400), angiitis with large multinucleated giant cells (C: HE stain, ×400), thickened blood vessel (D: HE stain, ×400), and presence of amyloid angiopathy (E: Dylon stain, ×400).

tumor enhancement or infection/inflammation (encephalitis). Cerebral angiography revealed neither eccentric narrowing of medium-sized vessels nor concentric narrowing, which are characteristic findings of vasculitis. Technetium-99m propylene amine oxime single photon emission computed tomography showed decreased cerebral blood flow (CBF) in the lesions. However, gallium scintigraphy revealed weak accumulation.

Peripheral white blood cell count was normal, but serum C-reactive protein (0.81 mg/dl) and soluble-interleukin-2 receptor (790 U/ml) levels were slightly increased. Cerebrospinal fluid analysis showed no abnormalities and cultures and cytology findings demonstrated negative findings.

The preoperative differential diagnosis included lymphoma (intravascular lymphoma), leukoencephalopathy (progressive multifocal leukoencephalopathy, viral encephalitis, autoimmune disease, etc.), acute disseminated encephalomyelitis, and vasculopathy/vasculitis.

Left frontal osteoplastic craniotomy under general anesthesia and cerebral biopsy (meninges, cortex, and white matter) were performed. The histological diagnosis was primary angiitis of the CNS, or granulomatous, giant cell, or isolated angiitis (Fig. 2A–C). Vessels showing primary angiitis of the CNS were concomitantly affected by amyloid angiopathy, characterized as markedly thickened eosinophilic walls with round profiles (Fig. 2D). Dylon staining confirmed amyloid deposition in the walls of most vessels (Fig. 2E), including all of the inflamed vessels, in the leptomeninges, and the cortical gray matter. In addition, some vessels showed fibrinoid necrosis with mild lymphocytic and histiocytic infiltrates.

Prednisone (50 mg/day) was administered. The patient's dementia gradually improved and she was able to speak again. The CBF abnormalities also resolved. She continued to take 5 mg oral prednisone daily. Substantial reversal of the MR imaging changes in the white matter was observed. The patient has been followed up for more than 2 years and no signs of relapse have been observed.

Discussion

Primary angiitis of the CNS is defined as vasculitis restricted to the small leptomeningeal and parenchymal arteries and veins without apparent systemic involvement. In our case, laboratory investigations demonstrated normal findings for autoantibodies. On the other hand, CAA is a disease of the elderly, characterized by the deposition of amyloids in the cortical and leptomeningeal vessels. The association of CAA with only vascular inflammatory changes ('vasculitis') is thought to be extremely rare. However, the coexistence of CAA and granulomatous angiitis has been reported in several cases and is well recognized. The amyloid proteins are reported to be β-protein and AL (amyloid protein derived from immunoglobulin light chains). Clinical and laboratory evidence of cerebral angiitis is present in some patients,[11] but not in others, and some patients present with radiological evidence of mass lesions.[2,5,7,9–11] Granulomatous angiitis of the CNS is defined histologically by granulomatous inflammation of the cerebral blood vessels. Different conditions such as infection and altered immune state may induce granulomatous angiitis, suggesting that granulomatous angiitis is not a unique disease but represents a nonspecific immune reaction to injury to the blood vessels induced by amyloid deposition.[4]

Primary angiitis of the CNS can present as a number of clinical patterns, but the three dominant features are usually encephalopathy, headache, and focal neurological signs to various degrees. The pattern of clinical presentation in the CAA and primary angiitis of the CNS groups is similar. The most common clinical features in cerebral vasculitis associated with CAA are changes in the mental status (confusion states, poor memory/concentration or impaired conscious level), often leading to frank dementia, headache, hallucinations, and seizures.[8]

Diagnostic imaging can be difficult in such patients. Cerebral vasculitis associated with CAA and vascular inflammation often appears as prominent white matter changes on computed tomography and MR imaging. The white matter changes result from a combination of vascular compromise ischemia, hemorrhage, edema, and atrophy. Angiography has low sensitivity and specificity, with an enormous number of inflammatory, metabolic, malignant, or other vasculopathies mimicking CNS vasculitis. In our case, preoperative imaging showed the typical cerebral vasculitis associated with CAA. However, the present diagnosis could not have been established without biopsy. Therefore, cerebral biopsy with histological confirmation remains the 'gold standard' for an accurate diagnosis.[11]

Untreated primary angiitis of the CNS inevitably progresses to death, often within a year of onset. However, the outcome for patients with cerebral vasculitis associated with CAA varies considerably. The administration of high dose corticosteroids is the mainstay treatment for

this disease. Cyclophosphamide is also given as an immunosuppressive therapy. The response rate to medical therapy in cerebral vasculitis associated with CAA is 60%, with spontaneous recovery in only 5%.[3] Autopsy evidence suggests that immunosuppressive treatment decreases the amyloid burden.[6] On the other hand, sustained or dramatic improvements are rarely observed.[8] Among six patients with histology-positive primary angiitis of the CNS, two died, one suffered severe disability, two had moderate disability, and one had minor disability. All had received steroid and/or further immunosuppression therapy with no clear pattern of response to the treatment. However, in the present patient, high dose prednisone treatment (50 mg/day), as the initial induction therapy, promoted the healing of the progressive vessel inflammation, and low dose prednisone (5 mg/day) also effectively prevented relapse for more than 2 years. The preoperative differential diagnosis included intravascular lymphoma. Therefore, biopsy was promptly performed. Cerebral vasculitis associated with CAA should be included in the differential diagnosis in elderly patients, because timely histological diagnosis and aggressive treatment are critical to the successful recovery of such patients.

Acknowledgments

We thank Drs. Keisuke Ishii and Takeshi Kubo (Oita University School of Medicine) for valuable discussions.

References

1) Abe T, Maruyama T, Nagai Y, Kamida T, Wakabayashi Y, Ishii K, Fujiki M, Kobayashi H: Severe postoperative vasculitis of the central nervous system in a child with arteriovenous malformation: case report. *Surg Neurol* 68: 317–321, 2007
2) Briceno CE, Resch L, Bernstein M: Cerebral amyloid angiopathy presenting as a mass lesion. *Stroke* 18: 234–239, 1987
3) Fountain NB, Eberhard DA: Primary angiitis of the central nervous system associated with cerebral amyloid angiopathy: report of two cases and review of the literature. *Neurology* 46: 190–197, 1996
4) Gray F, Dubas F, Roullet E, Escourolle R: Leukoencephalopathy in diffuse hemorrhagic cerebral amyloid angiopathy. *Ann Neurol* 18: 54–59, 1985
5) Le Coz P, Mikol J, Ferrand J, Woimant F, Masters C, Beyreuther K, Haguenau M, Cophignon J, Pepin B: Granulomatous angiitis and cerebral amyloid angiopathy presenting as a mass lesion. *Neuropathol Appl Neurobiol* 17: 149–155, 1991
6) Mandybur TI, Balko G: Cerebral amyloid angiopathy with granulomatous angiitis ameliorated by steroid-cytoxan treatment. *Clin Neuropharmacol* 15: 241–247, 1992
7) Murphy MN, Sima AA: Cerebral amyloid angiopathy associated with giant cell arteritis: a case report. *Stroke* 16: 514–517, 1985
8) Scolding NJ, Joseph F, Kirby PA, Mazanti I, Gray F, Mikol J, Ellison D, Hilton DA, Williams TL, MacKenzie JM, Xuereb JH, Love S: Abeta-related angiitis: primary angiitis of the central nervous system associated with cerebral amyloid angiopathy. *Brain* 128: 500–515, 2005
9) Tamargo RJ, Connolly ES Jr, McKhann GM, Khandji A, Chang Y, Libien J, Adams D: Clinicopathological review: primary angiitis of the central nervous system in association with cerebral amyloid angiopathy. *Neurosurgery* 53: 136–143, 2003
10) Wong SH, Robbins PD, Knuckey NW, Kermode AG: Cerebral amyloid angiopathy presenting with vasculitic pathology. *J Clin Neurosci* 13: 291–294, 2006
11) Yamada M, Itoh Y, Shintaku M, Kawamura J, Jensson O, Thorsteinsson L, Suematsu N, Matsushita M, Otomo E: Immune reactions associated with cerebral amyloid angiopathy. *Stroke* 27: 1155–1162, 1996

Address reprint requests to: Tatsuya Abe, M.D., Department of Neurosurgery, Oita University School of Medicine, 1–1 Idaigaoka, Hasama-machi, Yufu, Oita 879–5593, Japan.
e-mail: abet@med.oita-u.ac.jp

Clin Rheumatol (2010) 29:443–445
DOI 10.1007/s10067-009-1358-x

CASE REPORT

Successful treatment with tacrolimus of progressive interstitial pneumonia associated with amyopathic dermatomyositis refractory to cyclosporine

Masaru Ando · Eishi Miyazaki · Mari Yamasue · Yukiko Sadamura · Toshihiro Ishii · Ryuichi Takenaka · Takeo Ito · Shin-ichi Nureki · Toshihide Kumamoto

Received: 2 October 2009 / Accepted: 21 December 2009 / Published online: 4 February 2010

Abstract A 58-year-old male was admitted to our hospital because of periungual nailfold an erythema and erythematous rash on the dorsal joints of his hands and feet, but no muscle weakness. He was thus diagnosed to have amyopathic dermatomyositis. He had moderate hypoxemia and his chest computed tomography scans demonstrated bilateral ground-glass opacities, implicating complication with interstitial pneumonia. Therapy was initiated with pulsed methylprednisolone followed by high-dose corticosteroids, pulsed cyclophosphamide, and cyclosporine. The skin manifestations improved; however, the pulmonary infiltrates and hypoxemia deteriorated during the 2-month period of the treatment. The treatment was switched from cyclosporine to tacrolimus because of an inadequate clinical response to the therapy, and this resulted in the resolution of interstitial pneumonia. This case indicates that tacrolimus administration should be considered for patients with this life-threatening disorder when it is judged to be refractory to cyclosporine.

Keywords Amyopathic dermatomyositis · Interstitial pneumonia · Tacrolimus

Introduction

Progressive interstitial pneumonia associated with amyopathic dermatomyositis (ADM) has been reported to show poor a response to therapy and has high mortality [1]. Recent reports suggest that early administration of cyclosporine for this life-threatening condition provides a favorable prognosis for some patients, but not for all [2–5]. This report presents a case with progressive interstitial pneumonia associated with ADM refractory to a combination therapy with high-dose corticosteroids, pulsed cyclophosphamide, and cyclosporine, in which a switch from cyclosporine to tacrolimus resulted in the resolution of the interstitial pneumonia.

M. Ando (✉) · E. Miyazaki · M. Yamasue · Y. Sadamura · T. Ishii · R. Takenaka · T. Ito · S.-i. Nureki · T. Kumamoto
Department of Internal Medicine 3,
Oita University Faculty of Medicine,
Idaigaoka 1-1, Hasama,
Yufu, Oita 879-5593, Japan
e-mail: mando@med.oita-u.ac.jp

Case report

A 58-year-old male was admitted because of a 1 month history of dyspnea on effort, general fatigue, low grade fever, and rashes, including periungual nailfold erythema, Gottron's papules on the metacarpophalangeal joints, and erythema around the elbow and knee joints. A deep skin biopsy showed a perivascular inflammatory infiltrate containing numerous lymphocytes in the upper dermis, consistent with the characteristic histopathological changes associated with dermatomyositis. The white blood cell count was 15,300/μl with 89.2% neutrophils and C-reactive protein level was 0.68 mg/dl (<0.21 mg/dl). The antinuclear antibody titer was elevated (×160), but anti-histidyl-tRNA synthetase antibodies (anti-Jo-1) were not detected. The creatine kinase level was slightly elevated (502 IU/L: 62–287 IU/L) and the aldorase was normal (5.2 IU/L: 2.1–6.1 IU/L). No muscle weakness was noted, and electromyography did not detect any abnormal wave. No myositis was detected in the muscle biopsy specimens obtained from the biceps. Therefore, ADM was diagnosed based on the criteria by Sontheimer [1].

He had experienced exertional dyspnea for a month. Fine crackles were audible bilaterally. An arterial blood gas analysis revealed pH of 7.381, PaO_2 of 65.3 Torr, and

$PaCO_2$ of 40.7 Torr. The circulating level of KL-6, a marker of interstitial pneumonia, was elevated with a value of 1,300 U/ml (<500 U/ml). A chest roentgenogram revealed faint reticular shadow in both lower lung fields. Chest high-resolution computed tomography (HRCT) scans showed bilateral subpleural reticular opacity with ground-glass attenuation (Fig. 1a). Bronchoalveolar lavage fluid (BALF) contained 2.93×10^5 cells/ml with 31.3% lymphocytes and 19.3% neutrophils. A CD4/CD8 ratio was 0.98. Cultures of blood, urine, and BALF to detect bacteria, fungi, and mycobacteria were negative and serological tests for atypical pathogens including *Mycoplasma pneumoniae*, *Clamydia pneumoniae*, and *Legionella* were negative as were β-D glucan and cytomegalovirus antigenemia.

The patient was thus diagnosed to have interstitial pneumonia associated with ADM, and therapy was initiated with methylprednisolone pulse-therapy (1 g/day, intravenously for 3 days) followed by high-dose oral prednisolone (60 mg/day), cyclosporine, and monthly pulsed cyclophosphamide (500 mg, intravenously). A trough value of cyclosporine was maintained between 100 and 150 ng/ml. The administration of this treatment regimen for 2 months, improved the skin manifestations; however, the chest images gradually deteriorated with lung shrinkage in chest roentgenograms and increased ground-glass opacities with patchy consolidation in HRCT scans (Fig. 1b). Because of the progressive hypoxemia, the patient was forced to receive high-dose oxygen. The interstitial pneumonia was judged to be refractory to the combination therapy including cyclosporine; therefore, the decision was made to switch the immunosuppressant from cyclosporine to tacrolimus with the minimum serum levels maintained between 5–10 ng/ml. This resulted in the gradual improvement of arterial blood gasses and the infiltrates in chest images. The lung opacities were almost resolved after the 9 months of tacrolimus administration, when prednisolone was tapered to 17.5 mg daily (Fig. 1c), and oxygen inhalation was not needed even on exercise. The patient experienced a cytomegalovirus infection as an adverse event during the course of combination therapy including tacrolimus. The infection was diagnosed based on the detection of the virus by antigenemia and it was successfully treated with ganciclovir.

Discussion

Interstitial pneumonia associated with ADM often shows aggressive course leading to death [2]. The early administration of cyclosporine in combination with high-dose corticosteroids is usually capable of decreasing the mortality in this fatal complication of ADM [3, 4]; however, numerous patients have died of respiratory failure despite early administration of cyclosporine [5, 6]. In this case, a switch of the immunosuppressant from cyclosporine to tacrolimus resulted in the resolution of interstitial pneumonia. This is the first reported case of a patient being rescued by using tacrolimus for progressive interstitial pneumonia associated with ADM, which was resistant to the conventional immunosuppressive therapies.

The lymphocyte number in the BALF was increased in this patient, similar to that reported in the previous papers [3–5]. Therefore, activated T lymphocytes may play a role in the pathogenesis of ADM as well as classical dermatomyositis; therefore, cyclosporine, a potent T-cell inhibitor, is employed for the treatment of progressive interstitial

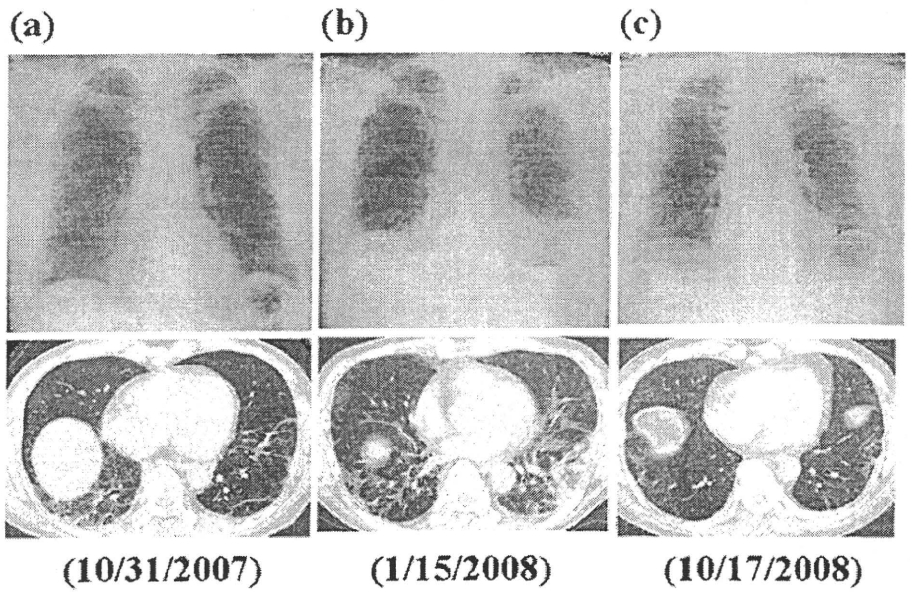

Fig. 1 **a** A chest roentgenogram on admission shows a faint reticular shadow in bilateral lower lung fields. Chest high-resolution computed tomography scans show bilateral subpleural reticular opacities with ground-glass attenuation. **b** A chest roentgenogram reveals increased reticular shadows with lung shrinkage during the 2 months of combination therapy including cyclosporine and the chest HRCT scans also show increased ground-glass opacities with patchy consolidation. **c** A chest roentgenogram and chest HRCT scans 9 months after the administration of tacrolimus show dramatic improvement of pulmonary infiltrates and shrinkage of the lung

pneumonia associated with ADM. However, previous papers disclosed that the efficacy of cyclosporine is limited [5, 6]. In this patient, a switch from cyclosporine to tacrolimus led to rescue the patient, indicating that tacrolimus may be superior to cyclosporine. Tacrolimus is a macrolide immunosuppressant with actions similar to those of cyclosporine, but the potency of tacrolimus in inhibiting in vitro T-cell activation and proliferation is up to 100 times greater than that of cyclosporine [7]. Although cyclosporine promotes the production of transforming growth factor, transforming growth factor beta (TGF-β) [8], tacrolimus reduces the TGF-β type I receptor expression on peripheral blood cells, followed by the inhibition of intracellular signal associated with TGF-β [9]. Moreover, the conversion from cyclosporine to tacrolimus induces the down-regulation of MCP-1 production in BALF [10], which has been elucidated to be one of the key chemokines in the pathogenesis of lung fibrosis [11]. These molecular mechanisms of tacrolimus may thus have led to the resolution of interstitial pneumonia in this case.

Although no cases with progressive interstitial pneumonia associated with ADM treated with tacrolimus were found in the literature, the drug has been used for patients with interstitial pneumonia associated with dermatomyositis (DM)/polymyositis (PM). Oddis et al. [12] treated five patients with anti-Jo-1 antibody-positive interstitial pneumonia and clinical improvement was obtained in three patients and disease stabilization was observed in another patient. Wilkes et al. [13] reported that DM/PM patients with refractory or severe interstitial pneumonia were all successfully treated with tacrolimus.

In summary, this case report suggests an alternative therapeutic option for progressive interstitial pneumonia associated with ADM refractory to cyclosporine. When interstitial pneumonia in ADM patients develops despite conventional immunosuppressive therapies including cyclosporin, a switch from cyclosporine to tacrolimus should be considered to rescue the patients. Further experience and clinical studies are therefore required to determine whether tacrolimus should be used prior to cyclosporine.

Disclosures None.

References

1. Sontheimer RD (2009) Would a new name hasten the acceptance of amyopathic dermatomyositis (dermatomyositis sine myositis) as a distinctive subset within the idiopathic inflammatory dermatomyopathies spectrum of clinical illness? J Am Acad Dermatol 46:626–636
2. Sontheimer RD, Miyagawa S (2003) Potentially fatal interstitial lung disease can occur in clinically amyopathic dermatomyositis. J Am Acad Dermatol 48:797–798
3. Miyazaki E, Ando M, Muramatsu T, Fukami T, Matsuno O, Nureki S, Ueno T, Tsuda T, Kumamoto T (2007) Early assessment of rapidly progressive interstitial pneumonia associated with amyopathic dermatomyositis. Clin Rheumatol 26:436–439
4. Shimojima Y, Ishii W, Kato T, Hoshi K, Matsuda M, Hashimoto T, Tanaka Y, Ikeda S (2003) Intractable skin necrosis and interstitial pneumonia in amyopathic dermatomyositis, successfully treated with cyclosporin A. Intern Med 42:1253–1258
5. Suda T, Fujisawa T, Enomoto N, Nakamura Y, Inui N, Naito T, Hashimoto D, Sato J, Toyoshima M, Hashizume H, Chida K (2006) Interstitial lung diseases associated with amyopathic dermatomyositis. Eur Respir J 28:1005–1012
6. Ideura G, Hanaoka M, Koizumi T, Fujimoto K, Shimojima Y, Ishii W, Matsuda M, Ikeda S (2007) Interstitial lung disease associated with amyopathic dermatomyositis: review of 18 cases. Respir Med 101:1406–1411
7. Siekierka JJ, Hung SH, Poe M, Lin CS, Sigal NH (1989) A cytosolic binding protein for the immunosuppressant FK506 has peptidyl-prolyl isomerase activity but is distinct from cyclophilin. Nature 341:755–757
8. Shihab FS, Andoh TF, Tanner AM, Noble NA, Border WA, Franceschini N, Bennett WM (1996) Role of transforming growth factor-beta 1 in experimental chronic cyclosporine nephropathy. Kidney Int 49:1141–1151
9. Baan CC, van Riemsdijk-van Overbeeke IC, Balk AH, Vantrimpont PM, Mol WM, Knoop CJ, Niesters HG, Maat LP, Weimar W (2001) Conversion from cyclosporin A to tacrolimus is safe and decreases blood pressure, cholesterol levels and TGF-beta 1 type I receptor expression. Clin Transplant 15:276–283
10. Meloni F, Cascina A, Paschetto E, Marone Bianco A, Morosini M, Pellegrini C, Fietta A, Vitulo P, Pozzi E, Vigano M (2003) Monocyte chemoattractant protein-1 levels in bronchoalveolar lavage fluid of lung-transplanted patients treated with tacrolimus as rescue treatment for refractory acute rejection. Transplant Proc 35:1523–1526
11. Wynn TA (2008) Cellular and molecular mechanisms of fibrosis. J Pathol 214:199–210
12. Oddis CV, Sciurba FC, Elmagd KA, Starzl TE (1999) Tacrolimus in refractory polymyositis with interstitial lung disease. Lancet 353:1762–1763
13. Fau Wilkes Mr, Sereika SM, Fau Sereika Sm, Fertig N, Fau FN, Lucas MR, Fau Lucas Mr, Oddis CV, Oddis CV (2005) Treatment of antisynthetase-associated interstitial lung disease with tacrolimus. Arthritis heum 52(8):2439–2446

Microbiology and Immunology

Microbiol Immunol 2010; **54**: 417–424
doi:10.1111/j.1348-0421.2010.00226.x

ORIGINAL ARTICLE

Increase of tumor necrosis factor-α in the blood induces early activation of matrix metalloproteinase-9 in the brain

Mitsuru Tsuge[1], Kozo Yasui[1], Takashi Ichiyawa[2], Yukie Saito[1], Yoshiharu Nagaoka[1], Masato Yashiro[1], Nobuko Yamashita[1] and Tsuneo Morishima[1]

[1]Department of Pediatrics, Okayama University, Graduate School of Medicine, Dentistry and Pharmaceutical Sciences, 2-5-1 Shikata-cho, Okayama, 700-8558, and [2]Department of Pediatrics, Yamaguchi University School of Medicine, 1-1-1 Minamikogushi, Ube, Yamaguchi, 755-8505, Japan

ABSTRACT

Increases of cytokine in the blood play important roles in the pathogenesis of influenza-associated encephalopathy. TNF-α was administered intravenously to wild-type mice, after which blood, CSF and brain tissue were obtained, and changes in BBB permeability, the amounts of MMP-9 and TIMP-1, and the localization of activated MMP were assessed. There was a significant increase in BBB permeability after 6 and 12 hr. MMP-9 was increased after 3 hr in the brain and cerebrospinal fluid, which was earlier than in the serum. TIMP-1 protein in the brain increased significantly after MMP-9 had increased. Activation of MMP-9 was observed in neurons in the cerebral cortex and hippocampus, and in vascular endothelial cells. These findings suggest that an increase in blood TNF-α promotes activation of MMP-9 in the brain, and may also induce an increase in permeability of the BBB. Early activation of MMP-9 in the brain may contribute to an early onset of neurological disorders and brain edema prior to multiple organ failure in those inflammatory diseases associated with highly increased concentrations of TNF-α in the blood, such as sepsis, burns, trauma and influenza-associated encephalopathy.

Key words blood-brain barrier, influenza associated encephalopathy, matrix metalloproteinase-9, tumor necrosis factor-alpha.

TNF-α is a pleiotrophic pro-inflammatory cytokine which is produced by various cells including activated monocytes, macrophages, B and T cells and fibroblasts. TNF-α plays a role in the induction of septic shock, autoimmune diseases, rheumatoid arthritis, inflammation and diabetes. TNF-α can change the permeability of the BBB where there is inflammation in the brain, as observed in meningitis (1), brain abscess (2) or brain ischemia (3).

MMP belong to a family of zinc-dependent proteolytic enzymes which are capable of degrading the components of the extracellular matrix in a variety of physiological and pathological conditions including embryogenesis, cell migration, tissue modeling, wound healing, and inflammation (4, 5). MMP are secreted as inactive pro-forms which are activated in proteolytic cascade reactions to yield active MMP. An uncontrolled increase in active MMP can result in tissue injury and persistent inflammation. MMP-9, a member of this enzyme family, is capable of degrading collagen IV, a major component of the basal membrane of the cerebral vascular endothelium, while also promoting a disruption of the BBB. MMP-9 is involved in acute brain injury such as cerebral ischemia (6–9), intracerebral hemorrhage (10, 11), neurodegenerative diseases (12, 13) and bacterial infections (14–16). In addition, MMP-9 is

Correspondence
Tsuneo Morishima, Department of Pediatrics, Okayama University, Graduate School of Medicine, Dentistry and Pharmaceutical Sciences, 2-5-1 Shikata-cho, Okayama, 700-8558, Japan.
Tel: +81 86 235 7247; fax: +81 86 221 4745; email: morishim@md.okayama-u.ac.jp

Received 24 November 2009; revised 8 March 2010; accepted 18 March 2010.

List of Abbreviations: BBB, blood-brain barrier; CSF, cerebrospinal fluid; DQ, dye-quenched; GFAP, glial fibrillary acidic protein; FITC, fluorescein isothiocyanate; IL-6, interleukin-6; IL-1β, interleukin-1β; MMP, matrix metalloproteinase; OCT, optimal cutting temperature; TIMP, tissue inhibitor of matrix metalloproteinase; TNF-α, tumor necrosis factor-alpha.

produced in the brain by several cell types, including endothelial cells, microglia, astrocytes, and neurons. MMP-9 activity is strictly regulated via gene transcription and dynamic inhibition by TIMP-1.

Acute encephalopathy, a severe complication of influenza infection in children, often results in severe brain edema and a grave prognosis (17). Several studies have demonstrated that concentrations of inflammatory cytokines, such as TNF-α, interleukin-6 and interleukin-1β, are increased in the serum or CSF of these patients (18–20). Interestingly, although neurological symptoms can occur at an early stage and a severe prognosis can easily follow, no influenza virus is found in the brain. Although these facts suggest that inflammatory cytokines are involved in the development of neurological injury in influenza-associated encephalopathy, the mechanism is still unclear. In the acute phase, serum concentrations of MMP-9 are much greater in influenza-associated encephalopathy than in influenza infection with no neurologic complications (21).

Although *in vitro* TNF-α can induce MMP-9 activation in various cells, such as macrophages, granulocytes, astrocytes, neurons, microglial cells, brain endothelial cells and choroid plexus epithelial cells, there have so far been no reports describing whether, *in vivo*, MMP-9 is actually activated in the brain in response to an increase of serum TNF-α. The current study evaluated time-dependent changes in the amount of MMP-9 in brain tissue, serum and CSF to determine the relationships between increases in serum TNF-α and activation of MMP-9 in the brain. In addition, under conditions of experimental hypercytokinemia with TNF-α *in vivo*, this study also showed changes in the brain in both TIMP-1 protein and localization of increased MMP.

MATERIALS AND METHODS

Animals

Eight-week-old male C57BL/6 mice weighing 25–30 g were obtained from Japan SLC, Shizuoka, Japan. The animals were housed in an air-conditioned room with a 12-hr light/dark cycle and free access to food and water. All procedures involving the animals were conducted in accordance with the Guidelines for Animal Experiments at Okayama University Advanced Science Research Center.

Treatment of animals and tissue preparation

One hundred μg/kg of murine recombinant TNF-α, IL-6 or IL-1β (Pepro Tech EC, London, UK) was injected intravenously into mice. Some mice were treated with saline as a vehicle control using the same volume and time schedule as for the cytokine treatments. The mice were deeply anesthetized with 1% halothane in 30% oxygen and 70% nitrous oxide using a face mask at 0, 3, 6, 12, 24 and 48 hr after the intravenous injection, and both blood and CSF quickly collected. They were then perfused transcardially with ice-cold PBS, after which their brains were quickly removed, divided into hemispheres, immediately frozen in liquid nitrogen, and stored at −80°C. After complete coagulation the blood samples were centrifuged at 3000 *g* for 10 min. The supernatants were collected and stored at −80°C. CSF samples were directly stored at −80°C.

Quantitative evaluation of extravasation of Evans blue

Vascular permeability was quantitatively evaluated using Evans blue dye. 2% Evans blue (Wako, Osaka, Japan) in saline was injected intravenously (4 ml/kg) as a BBB permeability tracer 1 hr prior to the termination of each time point ($n = 5$ per time point). The mice were killed one hr after this injection and then transcardially perfused with 100 ml of ice-cold PBS to remove the intravascular dye. The brains were removed, homogenized in 1 ml of 50% trichloroacetic acid, and then centrifuged (10 000 *g*, 20 min). A spectrophotometer was used to quantify the dye concentrations at 605 nm. The calculations were based on external standards (50–1000 μg/ml) dissolved in the same solvent. The amount of extravasated Evans blue was quantified as one microgram per gram of brain.

MMP inhibition *in vivo*

Intraperitoneal GM6001 (Calibiochem, San Diego, CA, USA) at 65 mg/kg or vehicle (1.5 ml of 10% dimethyl sulfoxide) was injected 1 hr before administration of TNF-α. Six hours after the administration of TNF-α, 2% Evans blue dye was injected intravenously and the brains dissected out 1 hr later.

Protein extraction

All procedures were carried out at 4°C. The brains were homogenized in a Polytron homogenizer (Paterson, NJ, USA) in 2 ml of working buffer (50 mM Tris-HCl, 150 mM NaCl, 5 mM $CaCl_2$, 1% Triton X-100, 0.05% BRIJ-35) and centrifuged, then the supernatants were stored at −80°C for further analysis. The total protein concentration was measured using the BCA protein assay kit (Pierce Biotechnology, Rockford, IL, USA). The total protein concentration of the serum samples was also measured using the same method.

ELISA

ELISA was used to measure the amounts of MMP-3, MMP-9 and TIMP-1 in order to detect the proteins that were expressed in the brain ($n = 5$ per time point). The MMP-9 assay recognizes both the pro- and active forms of MMP-9. Each capture antibody, the biotinylated detection antibodies, protein standards, and detection reagents for the ELISA were obtained from R&D Systems (Minneapolis, MN, USA).

Gelatin zymography

Equal amounts of prepared protein samples were diluted in twice the volume of sample buffer (125 mM Tris-HCl, 20% glycerol, 4% SDS, 0.003% bromophenol blue) without β-mercaptoethanol and were then loaded onto 10% SDS-PAGE gels containing 1% gelatin under non-reducing conditions. The gels were separated by electrophoresis at 4°C. After electrophoresis, the gels were washed twice for 20 min each in renaturing buffer containing 2.5% Triton X-100 at room temperature to remove any SDS, and were then incubated for 24 hr in developing buffer (10 mM CaCl2, 50 mM Tris, 50 mM NaCl) at 37°C. After incubation, the gel was stained for 1 hr with 0.5% Coomassie blue G-250 in 40% methanol and 10% acetic acid and was then destained in the same buffer without dye.

In situ gelatin zymography

In situ gelatin zymography was performed with DQ-gelatin-FITC (Molecular Probes, Eugene, OR, USA) on frozen fresh brain slices obtained from the mice. The brains were dissected out, immediately embedded in Tissue-Tek OCT compound (Sakura Finetechnical, Tokyo, Japan) and frozen on dry ice. Ten μm thick coronal sections were cut using a cryostat, and then air-dried for 30 min at room temperature, re-hydrated in PBS and incubated overnight at 37°C with 40 μg/ml of DQ-gelatin-FITC in PBS. Excess fluorogenic substrate was removed by washing three times in PBS. The brain slices were incubated with DQ-gelatin-FITC including the MMP inhibitor GM6001 (Calibiochem) to determine whether the gelatinolytic activity was due to matrix metalloproteinases. After *in situ* gelatin zymography had been done, immunohistochemistry was performed on the same brain sections to assess the cellular localization of gelatinases. Neurons were stained with NeuroTrace fluorescent Nissl stain solution (1:100; Molecular Probes), astrocytes with anti-GFAP antibody (1:200; Molecular Probes) and cerebral vascular endothelial cells with anti-claudin-5 H-52 antibody (1:100; Santa Cruz Biotechnology, Santa Cruz, CA, USA). After blocking with 2% BSA the sections were incubated for 20 min at room temperature with NeuroTrace fluorescent Nissl stain solution to stain the neurons. After washing in PBS, the sections were incubated for 2 hr at room temperature. The sections were treated with primary antibodies for astrocytes or vascular endothelial cells for 2 hr at 37°C after blocking. The sections were then washed in PBS, and incubated with secondary antibody solutions (anti-rabbit Alexa Fluor 594, 1:200; Molecular Probes) for 30 min at 37°C. Finally, the slides were washed in PBS and mounted on Vectashield mounting medium (Vector Laboratories, Burlingame, CA, USA). The tissue sections were photographed by fluorescence microscopy (Keyence BZ-9000) using the Keyence BZ-2 system (Keyence, Osaka, Japan).

Statistical analysis

All analyses were performed using the SPSS for Windows software package (SPSS, Chicago, IL, USA). Quantitative data were expressed as the mean ± d standard deviation. Statistical comparisons were conducted using ANOVA followed by the Tukey–Kramer tests for multiple comparisons. Differences with a P value of < 0.05 were considered to be statistically significant.

RESULTS

Quantitative evaluation of Evans blue extravasation

Changes in vascular permeability of the BBB were observed by measuring the amount of Evans blue leaking into the brain from the blood. Intravenous murine TNF-α induced a significant increase in Evans blue leaking outside the blood vessels 6, 12 and 24 hr later, in comparison to that found at the time of TNF-α injection ($P < 0.05$; Fig. 1). Intravenous saline as control produced no change in the amount of extravasated Evans blue up until 48 hr later. In comparison to the controls, significant increases in Evans blue extravasation were also seen both 6 and 12 hr after TNF-α injection ($P < 0.05$). Murine recombinant IL-6 and IL-1β administered in the same way had no effect on the amount of extravasated Evans blue into the brain 24 and 48 hr later (Fig. 2a, b).

Effect of MMP inhibition on Evans blue extravasation

GM6001 is a potent broad-spectrum inhibitor of matrix metalloproteinases and has been used in a number of animal models of disease where matrix metalloproteinases are thought to be involved. GM6001 solution was administered intraperitoneally prior to intravenous injection of TNF-α. Extravasated dye in the brain was measured 6 hr after injection of TNF-α. The amount of extravasated

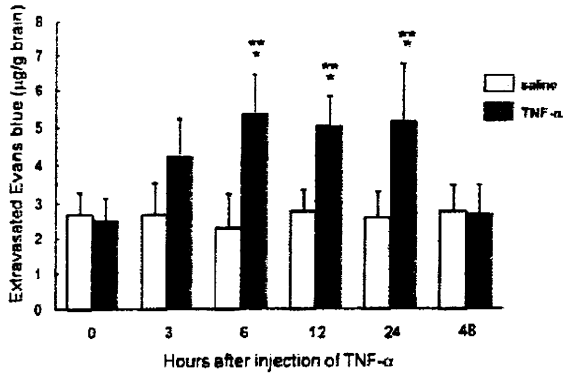

Fig. 1. Quantitative evaluation of Evans blue extravasation in the brain after intravenous injection of TNF-α (100 μg/kg). Extravasated Evans blue is expressed as μg/g of brain tissue. The values represent the mean ± standard deviation ($n = 5$ per time point). $^*P < 0.05$, in comparison to 0 hr after TNF-α administration; $^{**}P < 0.05$, in comparison to saline administration at the each time point.

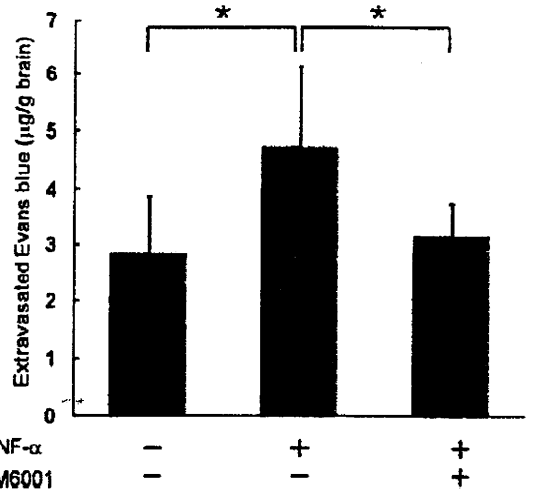

Fig. 3. Inhibition of the increase in Evans blue extravasation after intravenous injection of TNF-α (100 μg/kg) by intraperitoneal administration of an MMP inhibitor (GM6001). The values represent the mean ± standard deviation ($n = 8$ per time point). $^*P < 0.05$.

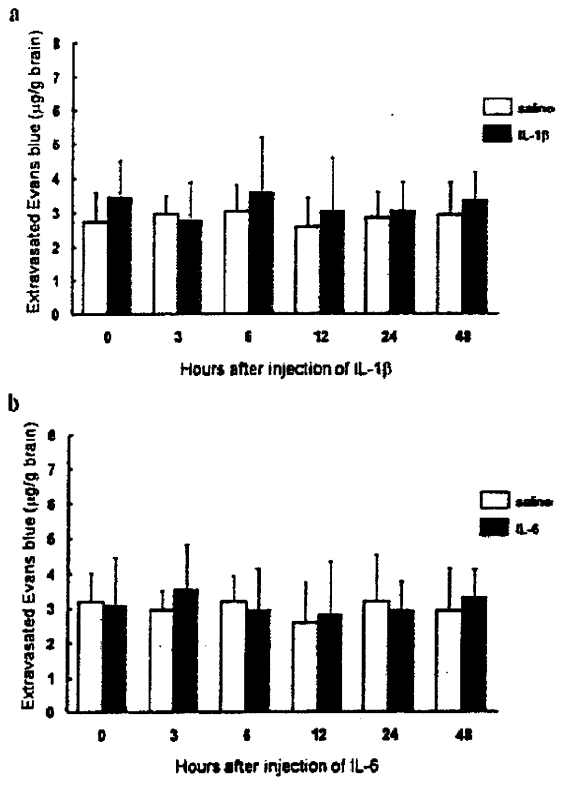

Fig. 2. Quantitative evaluation of Evans blue extravasation after intravenous injection of (a) IL-6 (100 μg/kg) and (b) IL-1β (100 μg/kg). The amount of extravasated Evans blue dye had not changed by 48 hr after the injection ($n = 5$ per time point).

dye was found to be significantly less in the brains of mice treated with GM6001 solution than in mice treated with solvent solution only ($P < 0.05$; Fig. 3).

MMP-3, MMP-9 and TIMP-1 protein in the brain

Time-dependent changes in MMP-9 and TIMP-1 proteins in the brain after TNF-α injection were evaluated using ELISA. The assay for MMP-9 was designed to measure total mouse MMP-9 (pro-MMP-9, active MMP-9 and TIMP-complexed MMP-9). MMP-9 protein in the brain was increased significantly at 3 hr post injection ($P < 0.01$), and gradually decreased thereafter (Fig. 4a). TIMP-1 protein in the brain was significantly increased at 12 hr post injection ($P < 0.01$), but had decreased significantly by 24 hr post injection (Fig. 4b). Time-dependent changes in MMP-3 protein in the brain were also evaluated using ELISA. MMP-3 protein was not detected in the brain (Fig. 4c). MMP-3 protein was detected from 0 to 48 hr in the serum, but was not significantly increased.

MMP-2 and MMP-9 in the brain, serum and CSF

After electrophoresis under non-reducing conditions, gelatin zymography classically produces two bands for murine MMP-2 (proenzyme and active forms; 72 and 65 kDa, respectively) and murine MMP-9 (proenzyme and active forms; 105 and 97 kDa, respectively) on the basis of molecular weight. Time-dependent changes in MMP-9 in the brain, serum and CSF were evaluated using

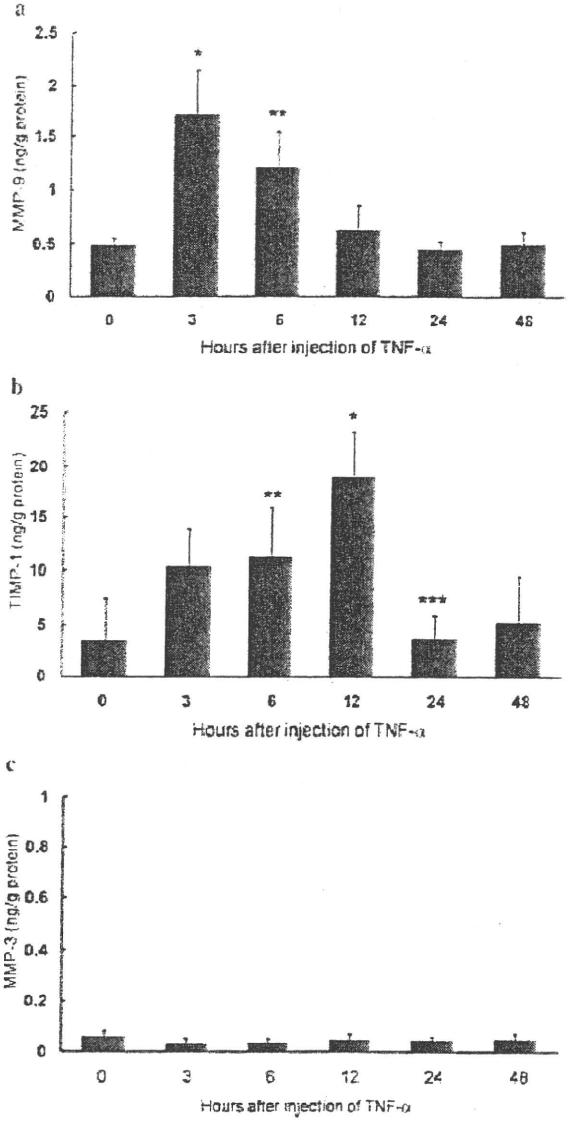

Fig. 4. Time-dependent changes in the amounts of (a) MMP-9, (b) TIMP-1 and (c) MMP-3 protein in the brain after intravenous injection of TNF-α as quantified by ELISA. The amount of each protein is expressed as ng/g of brain tissue. The values represent the mean ± standard deviation ($n = 5$ per time point). *$P < 0.01$, in comparison to at the time of TNF-α administration; **$P < 0.05$, in comparison to at the time of TNF-α administration; ***$P < 0.01$, in comparison to 12 hr after TNF-α administration.

gelatin zymography. MMP-9 increased predominantly in the active form in the brain, serum and CSF. The amounts of active MMP-9 in the brain and CSF peaked 3 hr after injection (Fig. 5). In comparison, the amount of active-MMP-9 in the serum was increased at 6 hr after injection. MMP-2 degrades gelatin as well as MMP-9. Active MMP-2 was continuously detectable in the brain and CSF from

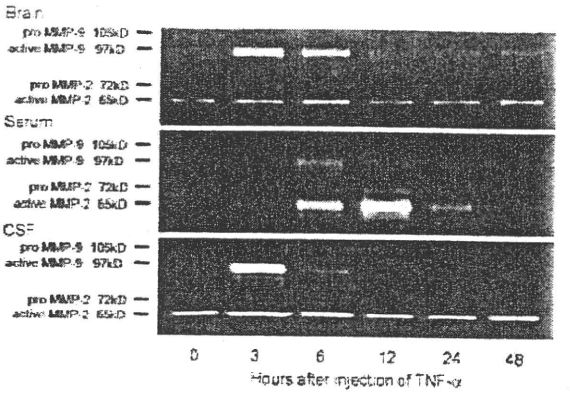

Fig. 5. Gelatin zymography after intravenous injection of TNF-α (100 μg/kg). Active MMP-9 was detectable in the brain, serum and CSF. MMP-9 increased transiently after the injection, and active MMP-9 in the brain and CSF were detected earlier than in the serum. MMP-2 was continuously detectable and demonstrated no significant change in the brain and CSF until 48 hr later, but MMP-2 increased in the serum at 6 and 12 hr post injection.

0 to 48 hr and did not seem to change significantly after administration of TNF-α. In contrast, both forms of MMP-2 were strongly detectable in the serum at 12 hr post injection. No other bands were detected by gelatin zymography.

Localization of gelatinases in the brain

MMP-9 can degrade not only collagen VI, but also gelatin. *In situ* gelatin zymography was used to determine in which parts of the brain gelatinases increased after TNF-α injection. After the brain had been put on gelatin labeled with FITC and incubated, the sites where there were activated gelatinases could be detected by the presence of digestion of the gelatin. We found that gelatinolytic activity was increased in the brain 3 hr later. In addition, *in situ* gelatin zymography with MMP inhibitor showed a decrease in most FITC signals (Fig. 6). Double staining with Nissl dye demonstrated that gelatinolytic activation was localized to the neurons of the cerebral cortex and hippocampus (Fig. 7). Activation was also detected in vascular endothelial cells by double staining with claudin-5. Astrocytes were found to come into contact with, or be surrounded by, cells that were positive for gelatinase activity, rather than being colocalized with this activity.

DISCUSSION

An increase in the vascular permeability of the BBB was induced by intravenous administration of murine recombinant TNF-α *in vivo*. Intracranial administration of TNF-α increases the permeability of the BBB *in vivo* (22). In